AD-A183 319 THE EFFECTS OF TEMPERATURE AND PRESSURE ON THE LONGITUDINAL VOLUME VISCOS..(U) CONNECTICUT UNIV STORRS INST OF MATERIALS SCIENCE B S HSIAO ET AL. 30 JUL 87 1/1

UNCLASSIFIED TR-3 N00014-86-K-0772 F/G 7/6 NL

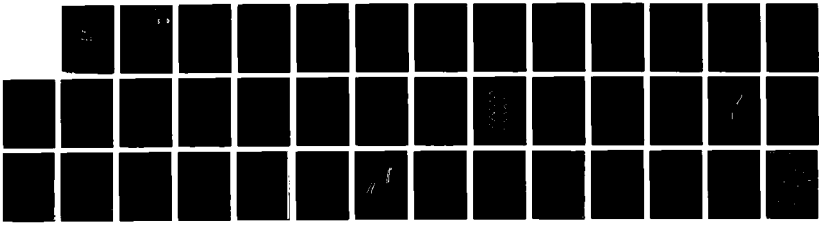

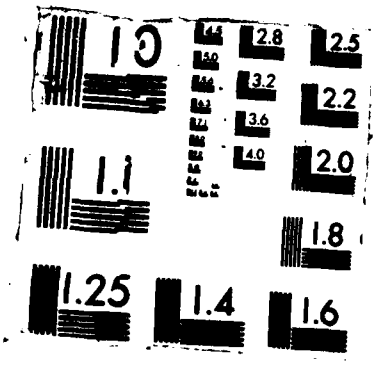
1.0
2.8
2.5
3.2
2.2
3.6
4.0
2.0
1.1
1.8
1.25
1.4
1.6

OFFICE OF NAVAL RESEARCH

CONTRACT NO. N00014-86-K-0772

TECHNICAL REPORT NO. 3

The Effects of Temperature and Pressure on the Longitudinal Volume Viscosity of Two Model Polymers

by

B. S. Hsiao, M. T. Shaw and E. T. Samulski

Prepared for Publication

in the

Journal of Rheology

Liquid Crystalline Polymer Research Center
Institute of Materials Science, U-136
The University of Connecticut
Storrs, CT 06268

July 30, 1987

Unclassified

SECURITY CLASSIFICATION OF THIS PAGE

AD-A183 319

REPORT DOCUMENTATION PAGE

1a REPORT SECURITY CLASSIFICATION: Unclassified	1b RESTRICTIVE MARKINGS: None
2a SECURITY CLASSIFICATION AUTHORITY	3 DISTRIBUTION / AVAILABILITY OF REPORT: Approved for Public Release, Distribution Unlimited
2b DECLASSIFICATION / DOWNGRADING SCHEDULE	
4 PERFORMING ORGANIZATION REPORT NUMBER(S): Technical Report No. 3	5 MONITORING ORGANIZATION REPORT NUMBER(S)
6a NAME OF PERFORMING ORGANIZATION: University of Connecticut; 6b OFFICE SYMBOL (If applicable)	7a NAME OF MONITORING ORGANIZATION: Office of Naval Research
6c ADDRESS (City, State, and ZIP Code): Institute of Materials Science, U - 136, 97 North Eagleville Road, Storrs, CT 06268	7b ADDRESS (City, State, and ZIP Code): 800 North Quincy Avenue, Arlington, VA 22217
8a NAME OF FUNDING / SPONSORING ORGANIZATION: Office of Naval Research; 8b OFFICE SYMBOL (If applicable): ONR	9 PROCUREMENT INSTRUMENT IDENTIFICATION NUMBER: N00014-86-K-0772
8c ADDRESS (City, State, and ZIP Code): 800 North Quincy Avenue, Arlington, VA 22217	10 SOURCE OF FUNDING NUMBERS: PROGRAM ELEMENT NO; PROJECT NO.; TASK NO.; WORK UNIT ACCESSION NO

11 TITLE (Include Security Classification)

The Effects of Temperature and Pressure on the Longitudinal Volume Viscosity of Two Model Polymers (Unclassified)

12 PERSONAL AUTHOR(S)

B. S. Hsiao, M. T. Shaw and E. T. Samulski

13a TYPE OF REPORT	13b TIME COVERED	14 DATE OF REPORT (Year, Month, Day)	15 PAGE COUNT
Interim	FROM 07/01/87 TO 07/31/87	1987-07-30	38

16 SUPPLEMENTARY NOTATION

Prepared for publication in the Journal of Rheology

17 COSATI CODES			18 SUBJECT TERMS (Continue on reverse if necessary and identify by block number)
FIELD	GROUP	SUB-GROUP	Longitudinal Volume Viscosity, Polysulfone, Polyethylene, Pressure effects on viscosity

19 ABSTRACT (Continue on reverse if necessary and identify by block number)

A method of studying dynamic longitudinal volume viscosity (η_l') at high pressure using a modified Instron capillary rheometer is demonstrated. Two model polymers were chosen as examples: an amorphous polysulfone and a semicrystalline high density polyethylene.

η_l' was measured at fixed pressure using a continuous temperature sweep. The pressure ranged up to 2000 bar, while temperatures were swept through the liquid to solid transition for each of the materials. The effects of frequency (from 0.0125 to 0.125 Hz) and strain (0.06 to 0.24%) on η_l' were also investigated. In both polymer systems, $|\eta_l'|$ increased as the pressure was increased or the frequency was decreased. (continued on reverse side)

20 DISTRIBUTION / AVAILABILITY OF ABSTRACT	21 ABSTRACT SECURITY CLASSIFICATION	
☒ UNCLASSIFIED/UNLIMITED ☒ SAME AS RPT ☐ DTIC USERS	Unclassified	
22a NAME OF RESPONSIBLE INDIVIDUAL: Dr. Kenneth J. Wynne	22b TELEPHONE (Include Area Code): (202) 696 - 4410	22c OFFICE SYMBOL: ONR

DD FORM 1473, 84 MAR — 83 APR edition may be used until exhausted. All other editions are obsolete.

SECURITY CLASSIFICATION OF THIS PAGE

Unclassified

19. ABSTRACT

In spite of the small strains employed, the viscosity was found to decrease as the strain was increased. The temperature-dependent η_i' varied with the nature of the transitions. In polysulfone, $|\eta_i'|$ decreased sharply with temperature above the T_g. However, in polyethylene, a positive dependence of $|\eta_i'|$ on temperature, limited to only a small temperature range above T_m, was observed. Under all conditions, $|\eta_i'|$ varied over the range 10^{12} to 10^{13} Pa.s, a much smaller change than found in η^*.

THE EFFECTS OF TEMPERATURE AND PRESSURE ON THE LONGITUDINAL VOLUME VISCOSITY OF TWO MODEL POLYMERS

Benjamin S. Hsiao, Montgomery T. Shaw and Edward T. Samulski

Institute of Materials Science

The University of Connecticut

Storrs, Connecticut 06268

SYNOPSIS

A method of studying dynamic longitudinal volume viscosity (η_L) at high pressure using a modified Instron capillary rheometer is demonstrated. Two model polymers were chosen as examples: an amorphous polysulfone and a semicrystalline high density polyethylene.

η_L was measured at fixed pressure using a continuous temperature sweep. The pressure ranged up to 2000 bar, while temperatures were swept through the liquid to solid transition for each of the materials. The effects of frequency (from 0.0125 to 0.125 Hz) and strain (0.06 to 0.24%) on η_L were also investigated. In both polymer systems, $|\eta_L^*|$ increased as the pressure was increased or the frequency was decreased. In spite of the small strains employed, the viscosity was found to decrease as the strain was increased. The temperature-dependent $|\eta_L^*|$ varied with the nature of the transitions. In polysulfone, $|\eta_L^*|$ decreased sharply with temperature above the T_g. However, in polyethylene, a positive dependence of $|\eta_L^*|$ on temperature, limited to only a small temperature range above T_m, was observed. Under all conditions, $|\eta_L^*|$ varied over the range 10^{12} to 10^{13} Pa.s, a much smaller change than found in η^*.

INTRODUCTION

Dynamic longitudinal volume viscosity (η_L^*) can be expressed by the equation:[1]

$$\eta_L^* = \frac{M^*}{i\omega} \qquad [1]$$

where M^* is the complex bulk longitudinal dynamic modulus, and ω is the radial frequency. In general, M^* is defined as the modulus measured under compression (or tension), where the deformation is one-dimensional. In this study, M^* was measured by the axial compression of a cylinder confined by a rigid cylindrical wall.

M^* is a combination of shear modulus (G^*) and bulk modulus (K^*), as given by

$$M^* = K^* + \frac{4}{3}G^* \qquad [2]$$

Therefore, η_L^* can be expressed by

$$\eta_L^* = \eta_K^* + \frac{4}{3}\eta^* \qquad [3]$$

The complex dynamic longitudinal volume viscosity is defined in the usual manner: $\eta_L^* = \eta_L' + i\,\eta_L''$, where η_L' is the viscous (in phase) component of η_L^* and η_L'' is the elastic (out of phase) component. One can calculate the dynamic bulk viscosity from η_L^* data using eq. (1) if shear viscosity of the material is known.

Aleman *et al.*[3-5] have recently studied the longitudinal volume viscosity (η_L) of epoxide prepolymers, poly (vinyl chloride) and poly (butylene terephthalate) with an Instron capillary rheometer. Assuming that polymer melts behaved similiarly to a Voigt-Kelvin element, they calculated η_L from the viscous component of the bulk volume modulus. They found that η_L increased with an increasing compression rate, increasing temperature and decreasing strain.

In this paper, a novel technique will be introduced to measure the dynamic longitudinal volume viscosity; this technique uses a capillary rheometer, an instrument available in most of the polymer laboratories. No assumption of Voigt-Kelvin behavior is necessary. The transient longitudinal volume viscosity measured by Aleman is expected to behave differently than the η_L^* found in this research.

It was of particular interest to investigate the behavior of η_L^* through transitions, namely, a second-order and a first-order transition. From a molecular standpoint, longitudinal volume viscosity reflects both local motions as well as motions associate with entanglements and cross-links of the polymer molecules. One would expect to see an inherent distinction of the η_L^* behavior through different transitions. It is thus conceivable that η_L^* could be used to identify the transitions at high pressures.

EXPERIMENTAL PROCEDURE

Apparatus

A modified Instron capillary rheometer was used in this study; a detailed description was given previously.[6] An APPLE II plus computer was adapted for system control and data acquisition, serving to collect sample temperature, heater temperature, volume change and pressure response, as well as to control the system temperature and pressure. In addition to measuring longitudinal volume viscosity, software was developed to conduct various other experiments, such as differential thermal analysis (DTA) and pressure-volume-temperature (P-V-T) analysis using temperature or pressure sweeps.

The maximum operating temperature of the modified capillary rheometer was 380°C, while the maximum pressure was 6000 bars (6 GPa). The heating rate of the experiment was programmable from 1° C/min to 10°C min and the cooling rate from 1°C min to 3° C min via software. The temperature along the heater barrel would be held to within ± 1°C. The accuracy of the pressure measurement was about 0.5% and that of the volume measurement about 0.1%. The data collected on the microcomputer were transfered to an IBM 3084 for further analysis.

Materials and Specimen Preparation

The chosen amorphous system was polysulfone (PSF). This particular polysulfone was purchased directly from Modern Plastics Co., Bridgeport CT, in the shape of a rod; it was identified as similar to Union Carbide's *P-1700 polysulfone*[8,9] by *NMR, FTIR*, solution viscosity and DSC analysis. This polysulfone is derived from bisphenol A and 4,4'-dichlorodiphenylsulfone. The glass transition temperature (T_g) of this PSF, measured via a Perkin Elmer DSC 2 at a heating rate of 5°C/min, was about 185°C. T_g was defined as the temperature corresponding to the first change in slope of the heat capacity thermogram. The PSF rods were machined down to the size of the inner diameter of the Instron barrel and vacuum dried at 140°C for 24 hours. Each rod weighed about 20 grams.

Semicrystalline high density polyethylene (HDPE) rods were supplied by AIN Plastics Co, N.Y.; its M_n is about 181,000 g/mole determined by GPC analysis calibrated with the polystyrene standards. The melting temperature (T_m) of this HDPE, measured at the heating rate of 5°C/min, was 135° C. T_m was taken as the peak temperature of DSC enthalpy thermogram. The crystallinity of this HDPE is approximately 82%. Specimens were prepared similarly to those made from PSF.

Rheological Measurements

Both materials' shear responses were characterized by a Rheometrics System 4. The dynamic shear modulus was measured at a fixed strain (0.24%), fixed frequency (1 Hz) and under negative temperature sweep to mimic the conditions typically used for bulk longitudinal volume viscosity runs. Two test fixtures were used, a parallel plate for the melts and a rectangular bar for the solid specimens.

For the bulk longitudinal viscosity measurements, the materials were first heated to the melt state at a rate of 3° C/min under high pressure. During the heating process, the high pressure DTA thermogram and P-V-T data could be gathered. This information was used to characterize the system at high pressure. After annealing at the first temperature for 30 minutes, data was taken as described below. It was anticipated that the annealing would erase the previous thermal history of the specimen. The specimen was cooled at a rate of 2°C/min to the next temperature, where it was held for 5 minutes before measurements were taken.

To measure η_L^*, a constant-frequency sawtooth volume deformation was applied to the specimen. A typical example of this volume deformation and its pressure response is shown in Figure 1. The data rate was typically 4 points per second.

Both pressure and volume responses were normalized by dividing by the average pressure (P_{ave}) and average volume (V_{ave}) respectively. P_{ave} and V_{ave} are the mean values of pressure and volume responses. To these normalized responses, Fourier series were fitted using IMSL subroutine FFTSC. This procedure is illustrated in Figure 2, where the normalized pressure and volume

responses are shown along with the fundamentals of the respective Fourier series. The magnitude of η_L^* was then calculated by:

$$|\eta_L^*| = \frac{\Delta P}{\Delta V} \frac{1}{V_{ave}} \frac{1}{\omega} = \frac{P_1}{V_1} \frac{P_{ave}}{\omega} \qquad [4]$$

where ΔP is the amplitude of the pressure fundamental, ΔV is the amplitude of the volume fundamental, P_1 is the amplitude of the fundamental of the Fourier series of the pressure response, V_1 is that for the volume and ω is the radial frequency. The viscous (in phase) part of η_L^* was then determined by:

$$\eta_L' = |\eta_L^*| \sin\delta \qquad [5]$$

where δ is the phase angle between the pressure and volume fundamentals.

In this study, four frequencies were investigated, namely 0.0125, 0.025, 0.0625 and 0.125 Hz; pressure was ranged from 500 bar to 2000 bar; and three strains were examined (0.06%, 0.12% and 0.24%). The strain referred here was the ratio of the volume change (ΔV) to the average volume (V_{ave}). These conditions covered approximately the capabilities of the instrument.

RESULTS AND DISCUSSIONS

Polysulfone

Temperature Effects

An example of the longitudinal volume viscosity vs. temperature response for PSF is shown in Figure 3. The upper curve is the magnitude of η_L^* ($|\eta_L^*|$) while the lower one is η_L'. For discussion, this curve can be divided into four regions. In region 1, at high temperature, a positive dependency of η_L' on temperature is exhibited. This effect has tentatively been assigned to a failure to achieve thermal or mechanical equilibrium at the beginning of the experiment. In region 2, the melt range, the influence of temperature on η_L^* is in the expected direction. A comparison of this dependence and the temperature dependence of steady shear viscosity (η_o) for PSF, published by Shaw and Miller,[9] is shown in Figure 4. $|\eta_L^*|$ has a smaller temperature dependence than η_o and η' (compare Figure 5 with Figure 3). In this region, η_L' dominates η_L^*, while the elastic contribution is small. The ratio of $|\eta_L^*|$ to $|\eta^*|$ is about 10^6. In region 3, the material passes through its T_g and $|\eta_L^*|$ approaches a plateau while η_L' passes through a maximum, as does η' (in Figure 5) or η_B'.[2] In region 4, the glass state, the response is primary elastic and insensitive to temperature. The peak temperature of η_L' in region 3 is assigned logically to the glass transition temperature (T_g') during the cooling process. It is observed that, under 2000 bar, this T_g' (242 °C) is lower than the T_g (292 °C) determined previously during a positive temperature sweep, which is not unexpected.

Pressure Effects

The effect of pressure on η_L^* is shown in Figure 6 ($|\eta_L^*|$ vs. T) and Figure 7 (η_L' vs. T). The pressures range from 500 bar to 2000 bar. According to these figures, $|\eta_L^*|$ increases as the pressure is increased, and the peak temperature of η_L' is shifted to higher temperatures. The shift rate was about 22° C/kbar, compared to a dT_g/dP rate of 45° C kbar found from P-V-T measurements.[6,8] All the T_g's are listed in Table 1. The glass temperatures, measured from both paths, are dependent on the thermal history and pressure effects on the specimens. These have been discussed before.[2]

Frequency Effects

In spite of the narrow achievable frequency range (0.0125 to 0.125 Hz), the influence of frequency on the components of η_L^* was found to be significantly negative. This can be seen in Figure 8 ($|\eta_L^*|$ vs. T) and Figure 9 (η_L' vs. T). Again, this behavior is similar to that of the complex shear viscosity. Because the components of η_L^* are approximately dependent on the inverse first power of frequency, the longitudinal modulus ($|M^*|$) of the solid is roughly constant. T_g' also increased slightly with frequency, an effect which has been confirmed in other polymers.[10]

Strain Effects

The influence of strain on η_L^* was determined by crossplotting η_L^* temperature sweeps taken at various fixed strains. The $|\eta_L^*|$ vs. strain response in Figure 10 shows a significant decrease of $|\eta_L^*|$ with strain; η_L' exhibited the same behavior. This observation confirms the reports of Aleman *et al.* that η_L increases with a decrease in the compression ratio (same as the strain). In the strain investigated (0.06 to 0.12%), one expects linear behavior for the shear response. It is believed that part of this nonlinearity is due to the inherently nonlinear relations between the pressure and volume, which will be discussed next, while the other part might be purely geometrical.

Intrinsic Nonlinearity

To demonstrate the nonlinear strain dependence of the longitudinal volume viscosity, we start the discussion with a general form of the linear stress-strain relation:[1]

$$\sigma_{ij} = \int_{-\infty}^{t} \{G(t-t')[\dot{\gamma}_{ij}(t') - \frac{1}{3}\Sigma\dot{\gamma}_{kk}(t')\delta_{ij}] + \frac{3}{2}K(t-t')[\frac{1}{3}\Sigma\dot{\gamma}_{kk}(t')\delta_{ij}]\}dt' \qquad [6]$$

For one-dimensional longitudinal deformation, $\gamma_{22} = \gamma_{33} = 0$, $\gamma_{11} = \gamma$ and $\sigma_{11} = \sigma_T$, where, σ_T is the total stress and equals to the negative of the pressure (the direction is opposite). Equation 6 can be then reduced to:

$$\sigma_T = \frac{2}{3}\int_{-\infty}^{t} G(t-t')\dot{\gamma}(t')dt' + \frac{1}{2}\int_{-\infty}^{t} K(t-t')\dot{\gamma}(t')dt' \qquad [7]$$

Since in the melt region, K(t) > > G(t), the following relation holds.

$$\sigma_T = \frac{1}{2}\int_{-\infty}^{t} K(t - t')\dot{\gamma}(t')dt' \qquad [8]$$

Assuming that the polymer melt behaves like a single Maxwell element,

$$K(t) = K_o e^{-\frac{t}{\tau}} \qquad [9]$$

Here K_o is a constant and τ is the relaxation time. Equation 8 and 9 can be combined, giving:

$$\sigma_T = \frac{1}{2}\int_{-\infty}^{t} K_o e^{-\frac{t}{\tau}}\dot{\gamma}(t')dt' \qquad [10]$$

Additionally, two assumptions were made to simplify the above relations. Firstly, τ was assumed to be a linear function of the pressure (P):

$$\tau = \alpha P + \tau_o \qquad [11]$$

and secondly, P was proportional to the strain, γ ($P \propto \gamma$), so that,

$$\tau = \alpha'\gamma + \tau_o \qquad [12]$$

Where α, $\alpha'$and τ_o are constants. Equation 10 can be expressed as

$$\sigma_T = \frac{1}{2}\int_{-\infty}^{t} K_o e^{-\frac{t - t'}{\alpha'\gamma - \tau_o}}\dot{\gamma}(t')dt' \qquad [13]$$

Using equation 13, we integrated numerically over the sawtooth strain history, knowing that the material was undeformed at $t < 0$. With the suitable constants (K_o, α' and τ_o) chosen, the pressure response was calculated and the reduced pressure was illustrated in Figure 11, where $\gamma(t)$ was a triangle longitudinal deformation, simulating the typical strain deformation in the experiment. This calculated pressure qualitatively resembled the experimental pressure responses in Figure 1. Utilizing the analytical procedures described previously, $|\eta_L^*|$ and η_L' were calculated from equation 13 at various strains. Not surprisingly, the results revealed a nonlinear strain dependence of the longitudinal volume viscosity. Both $|\eta_L^*|$ and η_L' decreased rapidly with increasing strain. Only at very low strains (< 0.0001) did the viscosity approach an asymptotic value.

In summary, it can be shown by making reasonable assumptions that the dynamic longitudinal volume viscosity will appear to be nonlinear because of the asymmetry of the pressure over the deformation cycle. Linear behavior is expected only at very low strains, whereas convenient experimental strains are beyond this region.

High Density Polyethylene

Temperature Effects

An example of the temperature response of the dynamic complex longitudinal volume viscosity of HDPE is shown in Figure 12. The upper curve is $|\eta_L^*|$ while the lower one is η_L'. From this figure it can be seen that the behavior of both components of η_L^* is distinctively different than that of the shear response shown in Figure 13. Again, the magnitude of longitudinal volume viscosity exhibited a much narrorer range than the equivalent shear properties.

For the purpose of discussion, Figure 12 can be divided into three regions. In region 1, the melt region, a different behavior is observed compared to that of PSF. As the temperature is lowered, $|\eta_L^*|$ remains almost constant until region 2, the melting transition, is reached. In region 2, the material passes through a minimum near its crystallization temperation and $|\eta_L^*|$ is found to decrease with decreasing temperature. This confirms Aleman *et al.*'s observation that temperature has a positive effect on the longitudinal volume viscosity. However our data indicate that this effect occurs near the crystallization transition temperature only. In region 3 (solid region), the behavior of $|\eta_L^*|$ is somewhat similiar to that of solid PSF, in that the viscous part (η_L') no longer dominates. However, unlike PSF, the elastic contribution increases rapidly as temperature decreases.

Pressure Effects

As with PSF, pressure had a positive effect on the longitudinal volume viscosity of HDPE. This is shown in the Figures 14 and 15, for $|\eta_L^*|$ and η_L' respectively. $|\eta_L^*|$ increased with increasing pressure and the minimum was shifted to higher temperature by pressure. This shift rate was about 10°C/min, which is lower than the shift rate of the melting point due to pressure.[41]. The

crystallization temperatues and the melting temperatures are listed in Table 2. The pressure dependencies of the above transition temperatures again are different.

Frequency Effects

Figures 16 and 17 display the effect of frequency on $|\eta_L^*|$ and η_L' respectively. It was observed that both components of η_L^* decreased with increasing frequency. This behavior was similar to that of PSF. The crystallization temperatures appeared to be insensitive to frequency. In the solid-state region, frequency had a negative effect on $|\eta_L^*|$; again, $|M^*|$ (longitudinal bulk volume modulus) remained about constant.

Strain Effects

The strain dependence on the longitudinal volume viscosity of HDPE was examined by cross-plotting the $|\eta_L^*|$ vs. temperature diagrams at various fixed strains. The result is shown in Figure 18. From this figure, it can be seen that a negative correlation exists between strain and both components of η_L^* . This once more indicated that a intrinsic nonlinearity exists in the longitudinal volume viscosity. Aleman and his coworkers have reported a similar strain effect .[3,4,5]

CONCLUSIONS

In this paper, a modified Instron capillary rheometer was used to measure the complex dynamic longitudinal volume viscosity (η_L^*) of polymers. Two model polymer systems were investigated: an amorphous polysulfone and a semi-crystalline high density polyethylene. In both systems, all components of η_L^* increased with pressure, and decreased with frequency and strain. The negative strain dependence of η_L^* at very low strains could be explained as an artifactual consequence of the geometry. The two materials exhibited different behavior near their transitions. In PSF, temperature had a negative effect on both components of η_L^* , resembling the behavior of the complex dynamic shear viscosity (η^*) in polymer melts. A maximum of η_L' corresponded to the glass temperature. In HDPE, a positive temperature effect was observed just above the transition temperature region. A minimum in η_L' was observed, corresponding to the crystallization temperature of HDPE.

ACKNOWLEDGEMENT

Financial support for this research by the DARPA ONR Contract #N0014-86-K-0772 is greatly acknowledged.

FIGURE CAPTIONS

Figure 1. Volume deformation and the corresponding pressure response of HDPE at of 150°C.

Figure 2. The normalized volume and pressure responses along with their Fourier series' fundamentals.

Figure 3. The longitudinal volume viscosity vs. temperature diagram of PSF. The pressure is 2000 bar, frequency is 0.0625 Hz and strain is 0.24%. The upper curve is $|\eta_L^*|$ and the lower one is η_L'.

Figure 4. Temperature dependence of $|\eta_L^*|$ in Figure 3, compared with that of η_o, calculated from the Arrhenius relationship for PSF published by Shaw and Miller.[9]

Figure 5. Shear modulus against temperature diagram for PSF. The strain is 0.24%, frequency is 1 Hz. The upper curve is $|\eta^*|$ and the lower one is η'.

Figure 6. The pressure dependence of $|\eta_L^*|$ for PSF. The strain is 0.24% and frequency is 0.0625 Hz.

Figure 7. The pressure dependence of η_L' for PSF. The strain is 0.24% and frequency is 0.0625 Hz.

Figure 8. The effect of frequency on $|\eta_L^*|$ for PSF. The pressure is 2000 bar and strain is 0.12%.

Figure 9. The effect of frequency on η_L' for PSF. The pressure is 2000 bar and strain is 0.12%.

Figure 10. The effect of strain on $|\eta_L^*|$ for PSF. The pressure is 1500 bar and frequency is 0.0625 Hz.

Figure 11. Reduced pressure responses calculated by equation 14, where $\gamma(t)$ is a triangle deformation, and frequency = $0.625s^{-1}$, strain = 0.0012, K_o = $1x10^{-1}$ Pa, α' = $0.125x10^{6}s$, P_{max} = $1x10^{8}Pa$, τ_o = $5s$

Figure 12. The longitudinal volume viscosity vs. temperature diagram of HDPE. The pressure is 1000 bar, frequency is 0.0625 Hz and strain is 0.24%. The upper curve is $|\eta_L^*|$ and the lower one is η_L'.

Figure 13. Shear modulus vs. temperature diagram for HDPE. The strain is 0.24%, frequency is 1 Hz. The upper curve is $|\eta^*|$ and the lower one is η'.

Figure 14. The pressure dependence of $|\eta_L^*|$ for HDPE. The strain is 0.24% and frequency is 0.0625 Hz.

Figure 15. The pressure dependence of η_L' for HDPE. The strain is 0.24% and frequency is 0.0625 Hz.

Figure 16. The effect of frequency on $|\eta_L^*|$ for HDPE. The pressure is 1000 bar and strain is 0.06%.

Figure 17. The effect of frequency on η_L' for HDPE. The pressure is 1000 bar and strain is 0.06%.

Figure 18. The effect of strain on $|\eta_L^*|$ for HDPE. The pressure is 1000 bar and frequency is 0.0625 Hz.

REFERENCES

1. J. D. Ferry, "Viscoelastic Properties of Polymers", Wiley, New York. Third Edition (1980)

2. R. S. Marvin and J. E. Mckinney, *Physical Accoustics* , edited by W. P. Mason, Volume IIB, Academic Press, New York (1965)

3. P. Lesbats, R. Legros and J. V. Aleman, *J. of Polym. Sci. (Polym. Chem. Ed.)*, 20 , 1971-1984 (1982)

4. M. Sanchez-Sancha and J. V. Aleman, *Rheol. Acta*, 23 , 23-41 (1984)

5. M. Sanchez-Sancha and J. V. Aleman, *J. of Rheol.* 29(3) , 307-321 (1985)

6. B. S. Hsiao, M. T. Shaw and E. T. Samulski, *SPE ANTEC Tech. Paper*, 32 , 424-428 (1986)

7. B. S. Hsiao, M. T. Shaw and E. T. Samulski, *Rev. Sci. Instr.* in press (1987)

8. P. Zoller, *J. Polym. Sci. (Polym. Phys. Ed.)*, 16 , 1261-1275 (1978)

9. M. T. Shaw and J. C. Miller, *Polym. Eng. Sci.* 18(5) , 372 (1978)

10. E. N. Dalal and P. J. Phillips, *Macromolecules* 16 , 890 (1983)

11. K. D. Pae and S. K. Bhateja *J. Macromol. Sci. Rev. Macromol. Chem.* C13 , 1 (1975)

Table 1. T_g's measured in PSF

Pressure (bar)	T_g(HPDTA) (°C)	$T_g'(\eta_L')$ (°C)
500	222	210
1000	246	220
1500	269	232
2000	292	242

1. T_g(HPDTA): T_g measured from high pressure differential thermal analysis
2. $T_g'(\eta_L')$: T_g measured from longitudinal volume viscosity

Table 1. T_m and T_c measured in HDPE

Pressure (bar)	T_m(HPDTA) (°C)	$T_c(\eta_L')$ (°C)
1	135	-
1000	162	150
2000	182	156
3000	202	-

1. T_m(HPDTA): T_m measured from high pressure thermal analysis
2. $T_c(\eta_L')$: T_c measured from longitudinal volume viscosity

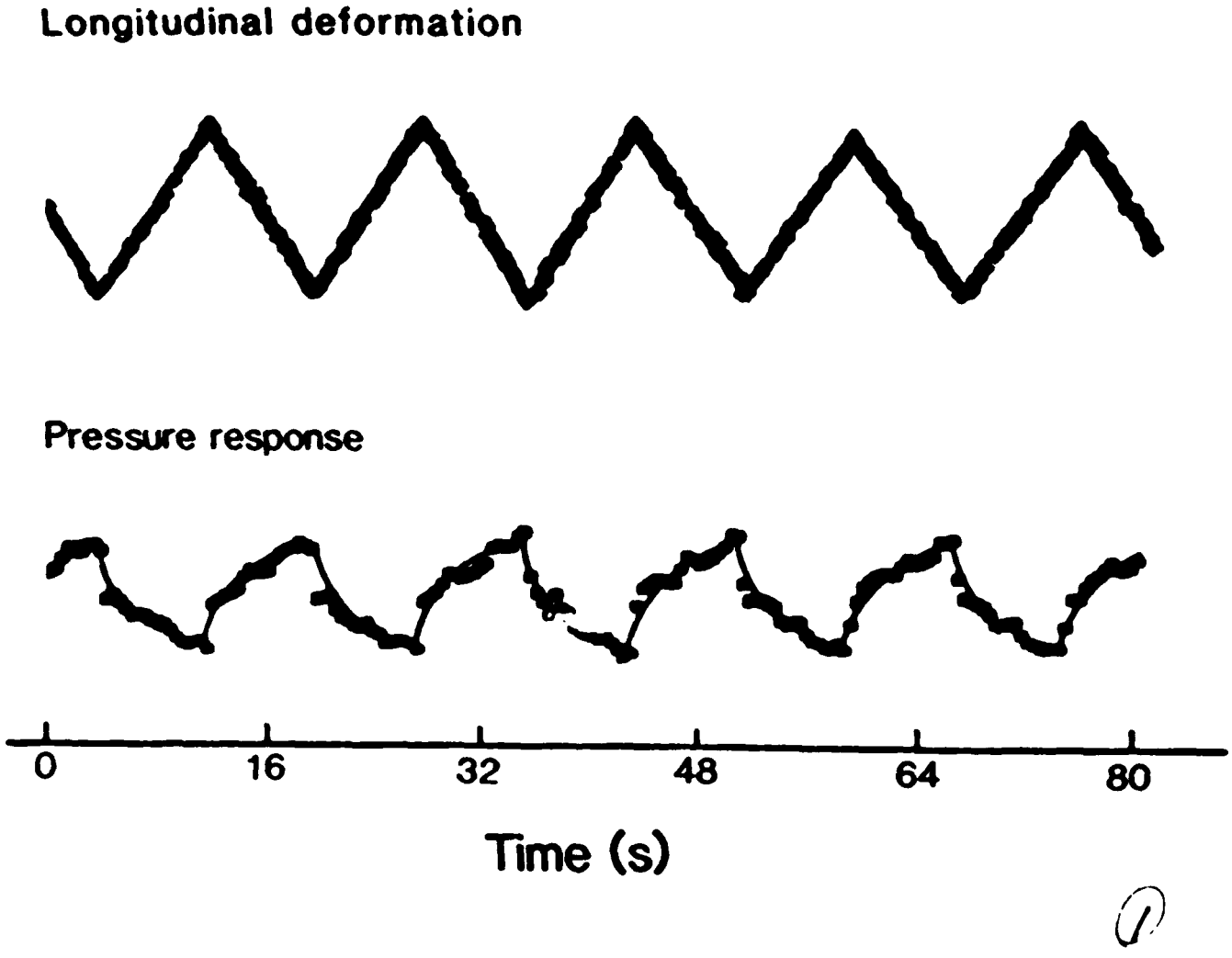
Longitudinal deformation
Pressure response
0
16
32
48
64
80
Time (s)

Longitudinal deformation

Pressure response

Fundamentals of Fourier series'

Volume

Pressure

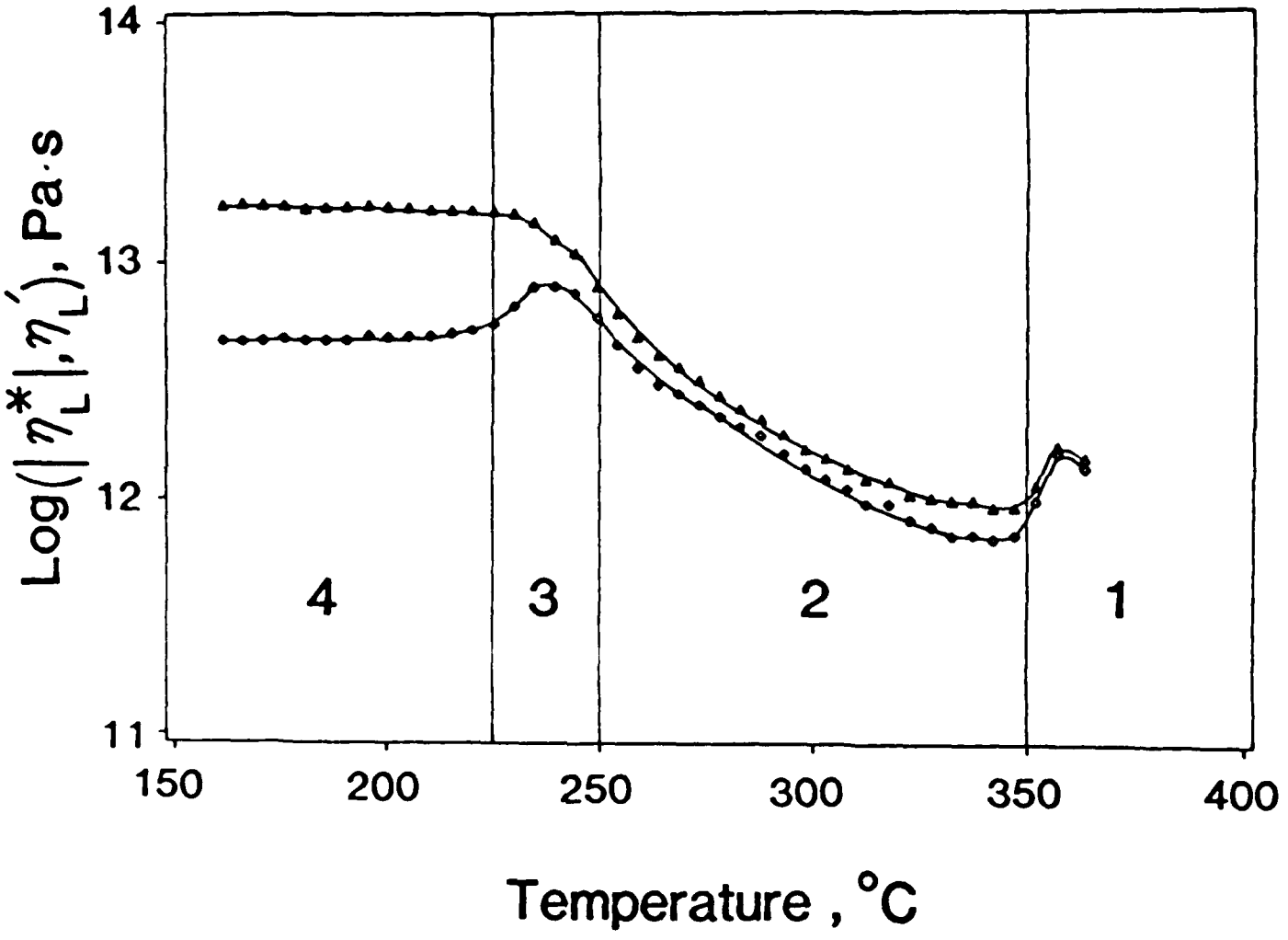
14
13
12
11
Log(|η*L|,η'L), Pa·s
4
3
2
1
150
200
250
300
350
400
Temperature , °C

(3)

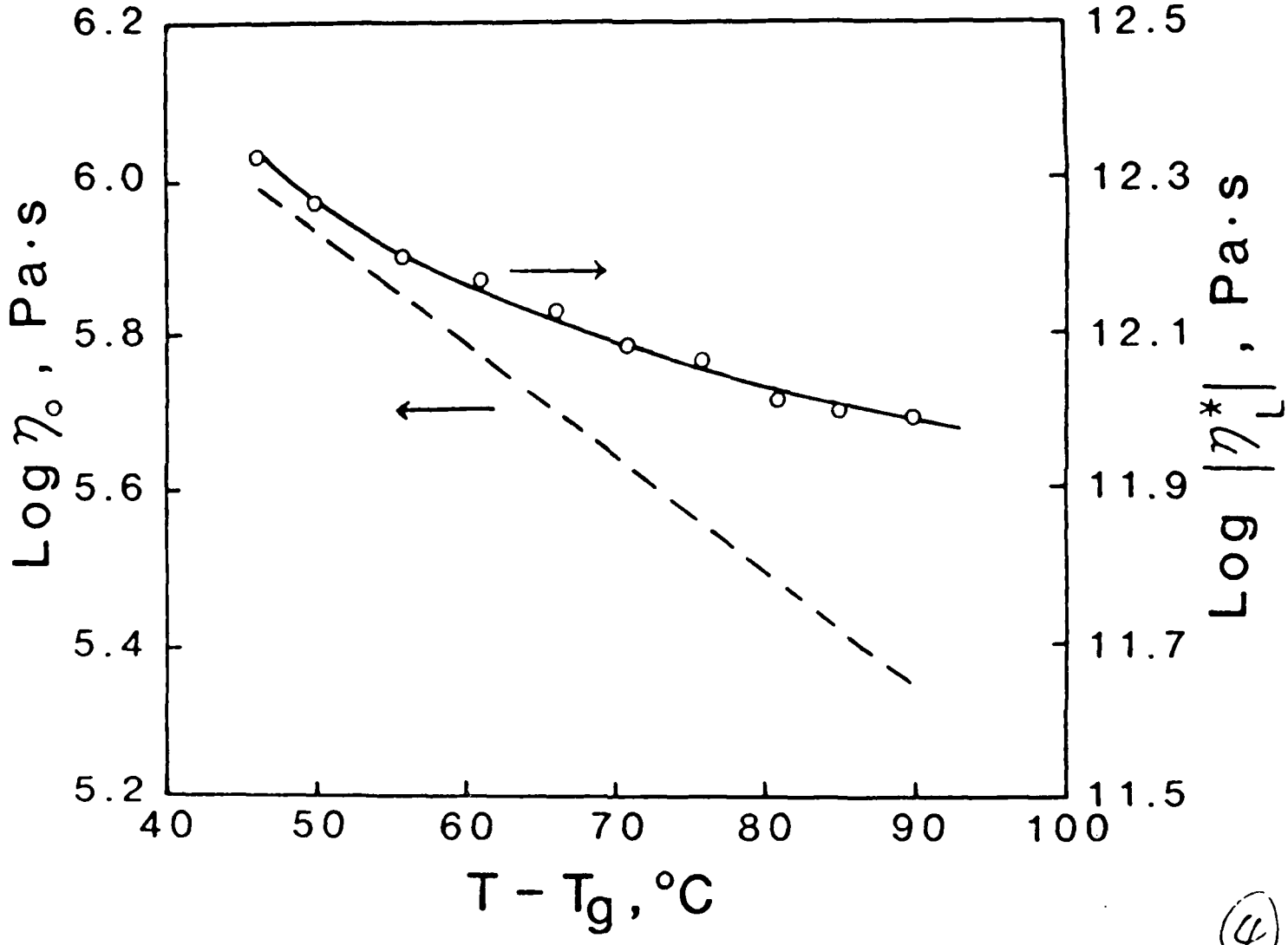
6.2
6.0
5.8
5.6
5.4
5.2
Log η_o , Pa·s
12.5
12.3
12.1
11.9
11.7
11.5
Log $|\eta^*_L|$, Pa·s
40
50
60
70
80
90
100
T – T_g , °C

(4)

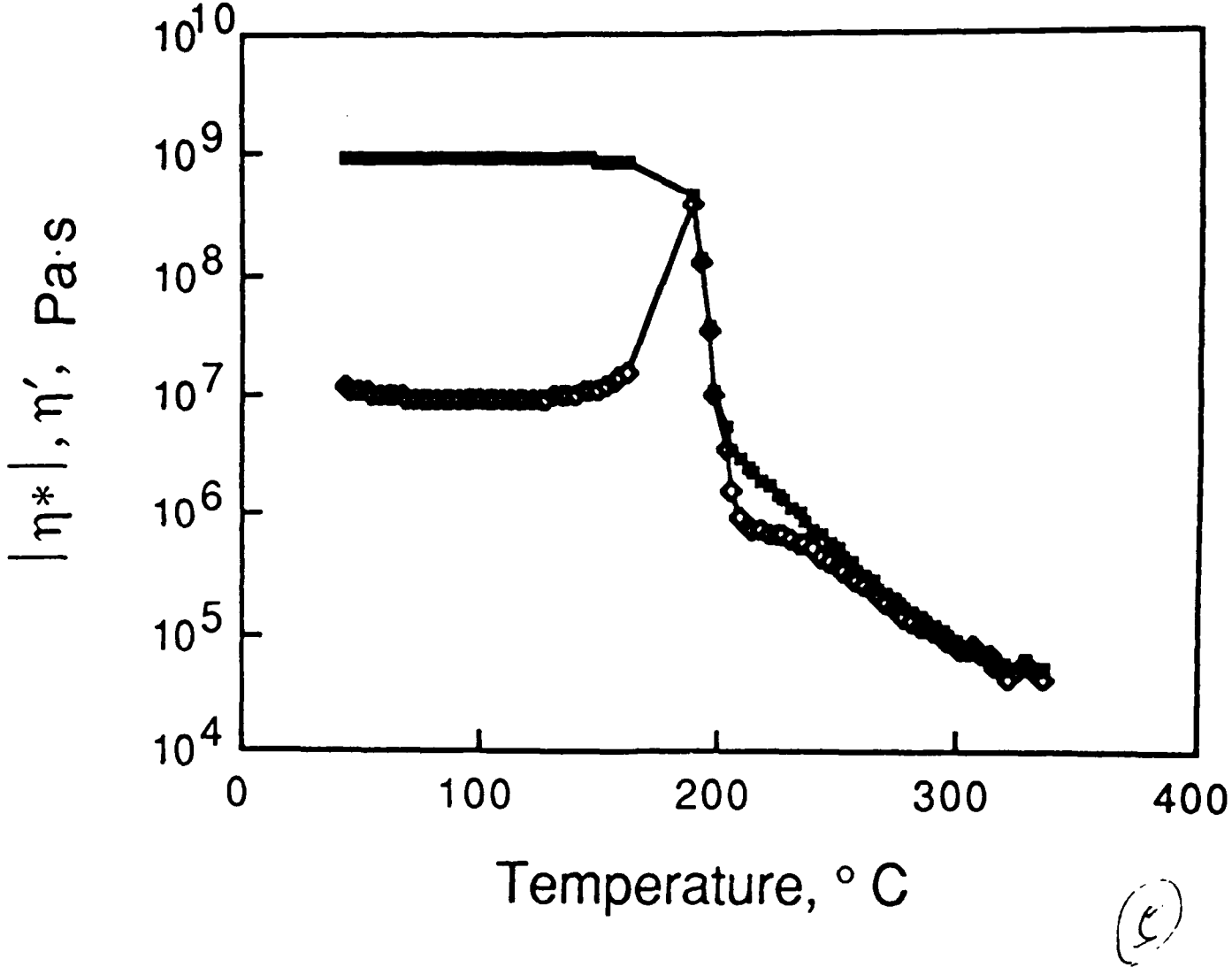
10^{10}
10^{9}
10^{8}
10^{7}
10^{6}
10^{5}
10^{4}
$|\eta^*|, \eta'$, Pa·s
0
100
200
300
400
Temperature, ° C

(ع)

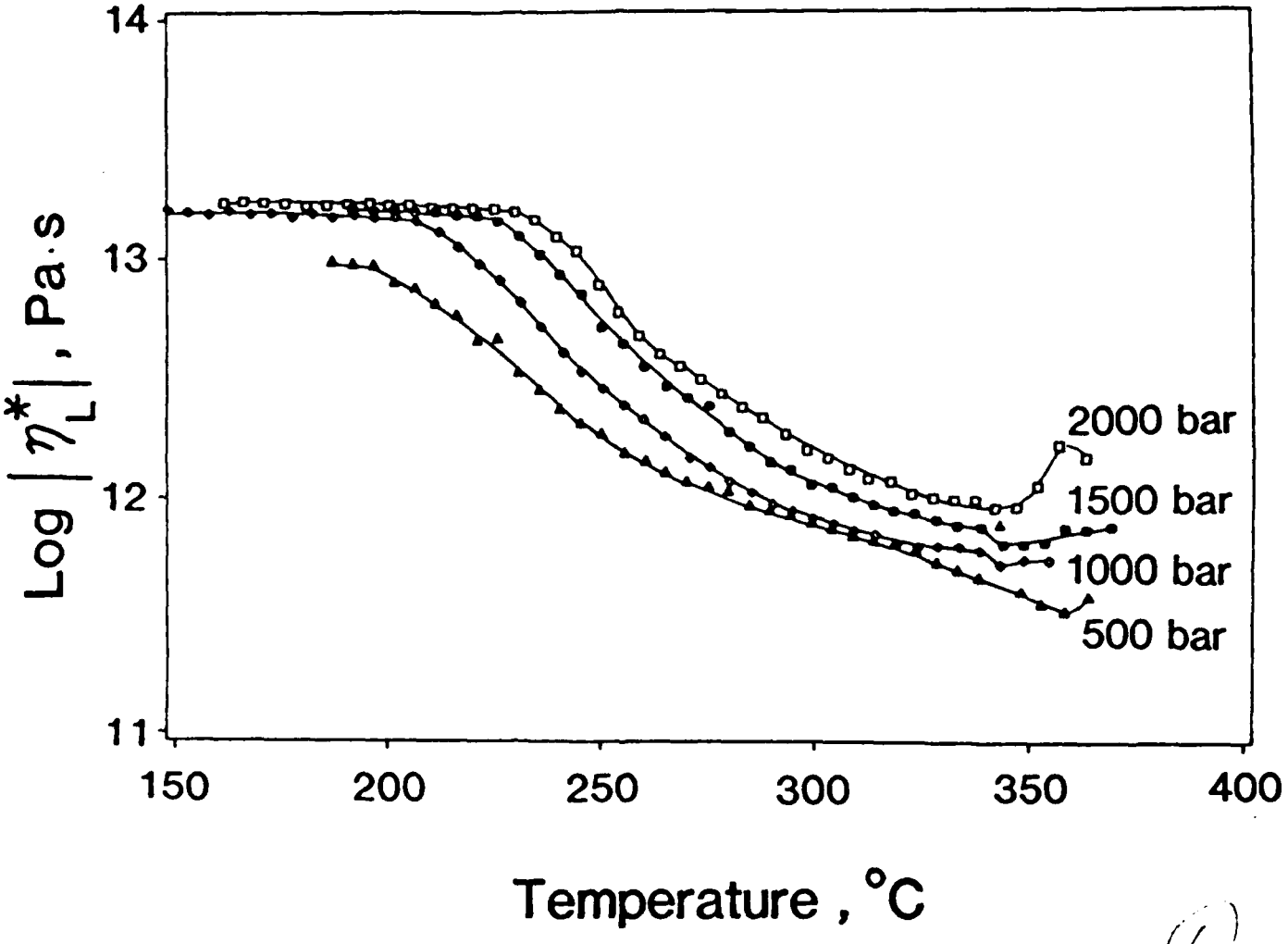
14
13
12
11
Log |η*L|, Pa·s
150
200
250
300
350
400
Temperature , °C
2000 bar
1500 bar
1000 bar
500 bar

(6)

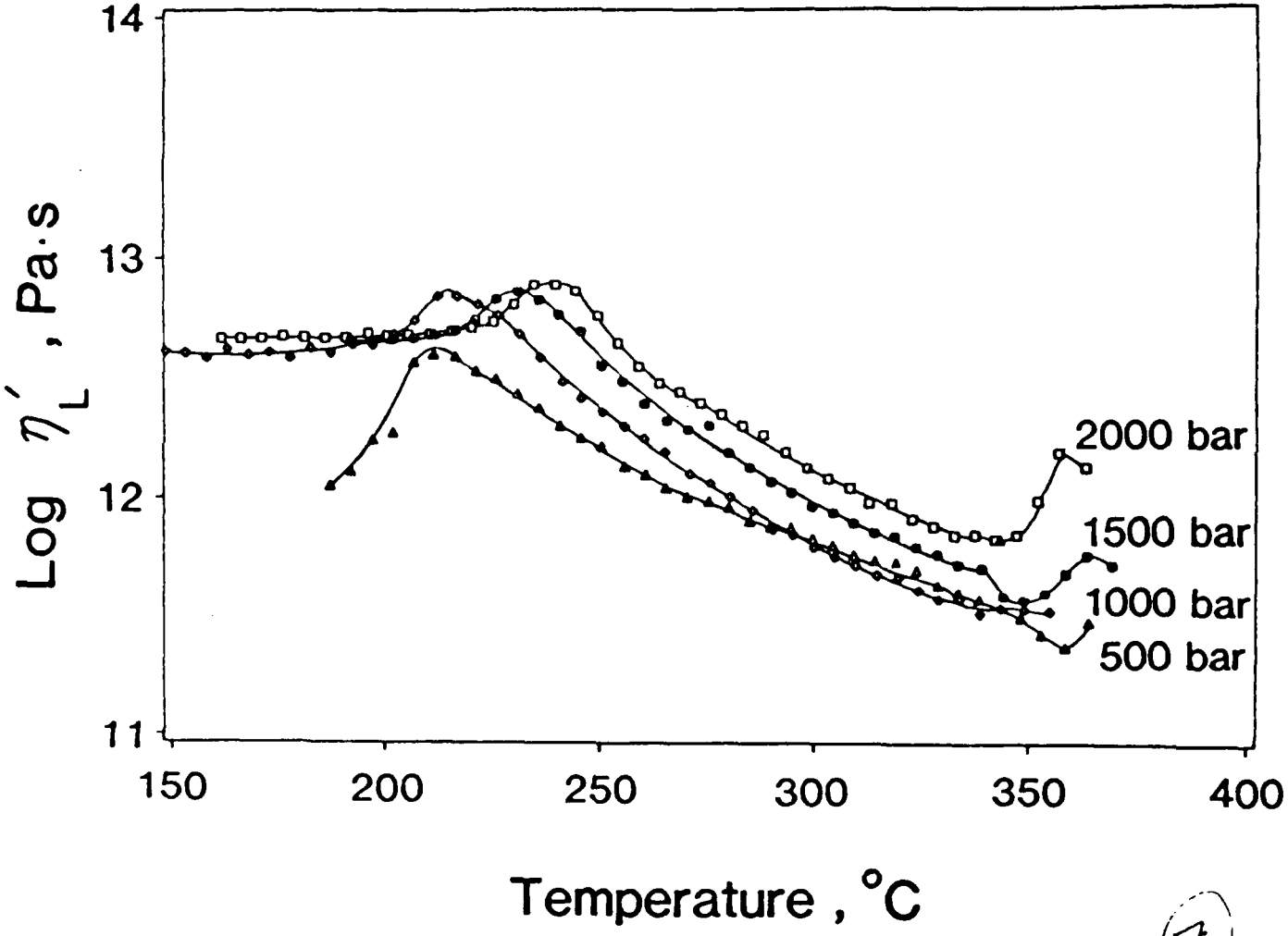
14
13
12
11
Log η_L' , Pa·s
150
200
250
300
350
400
Temperature , °C
2000 bar
1500 bar
1000 bar
500 bar

(7)

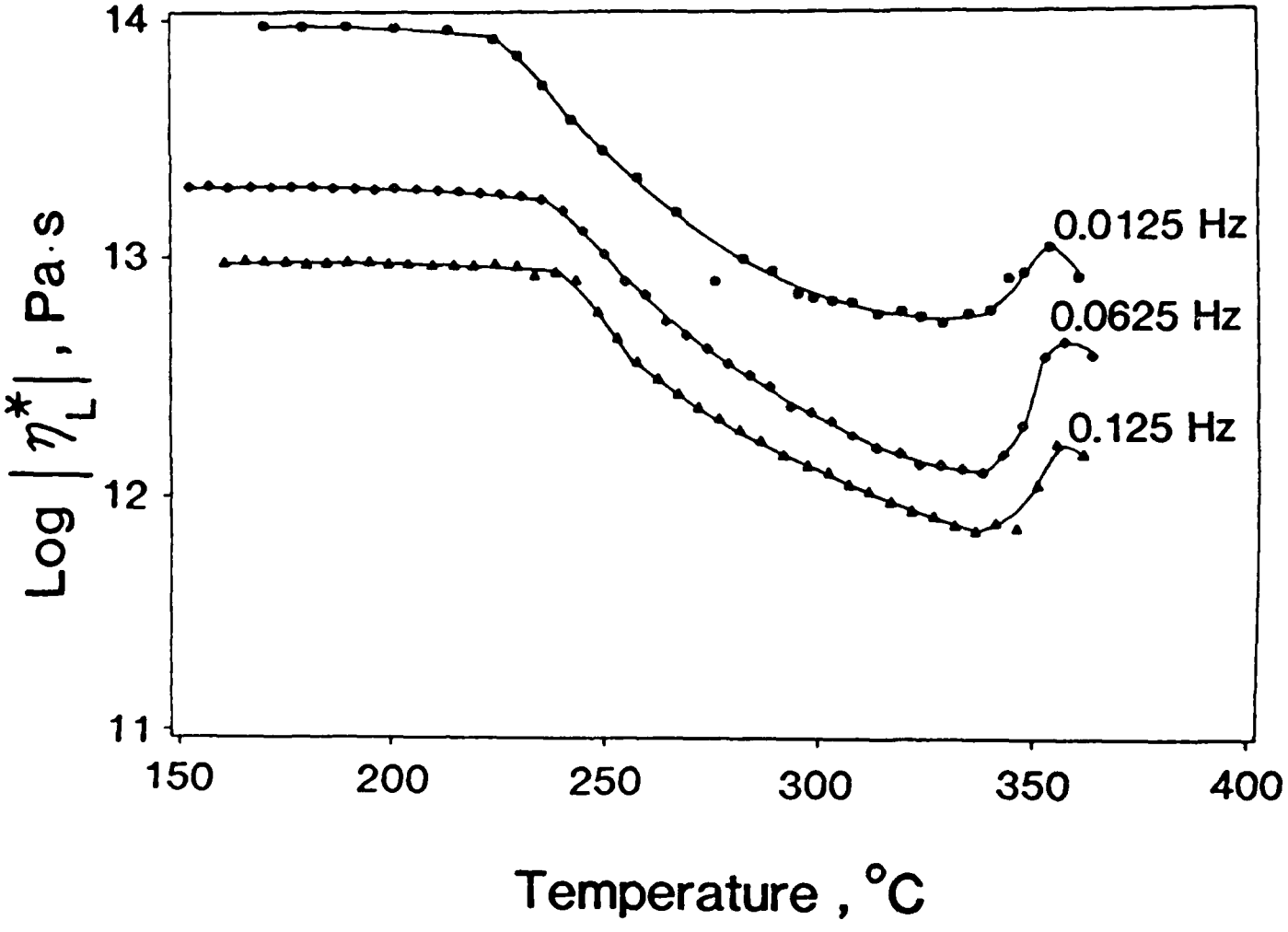
14
13
12
11
150
200
250
300
350
400
Log | η_L^* | , Pa·s
Temperature , °C
0.0125 Hz
0.0625 Hz
0.125 Hz

(8)

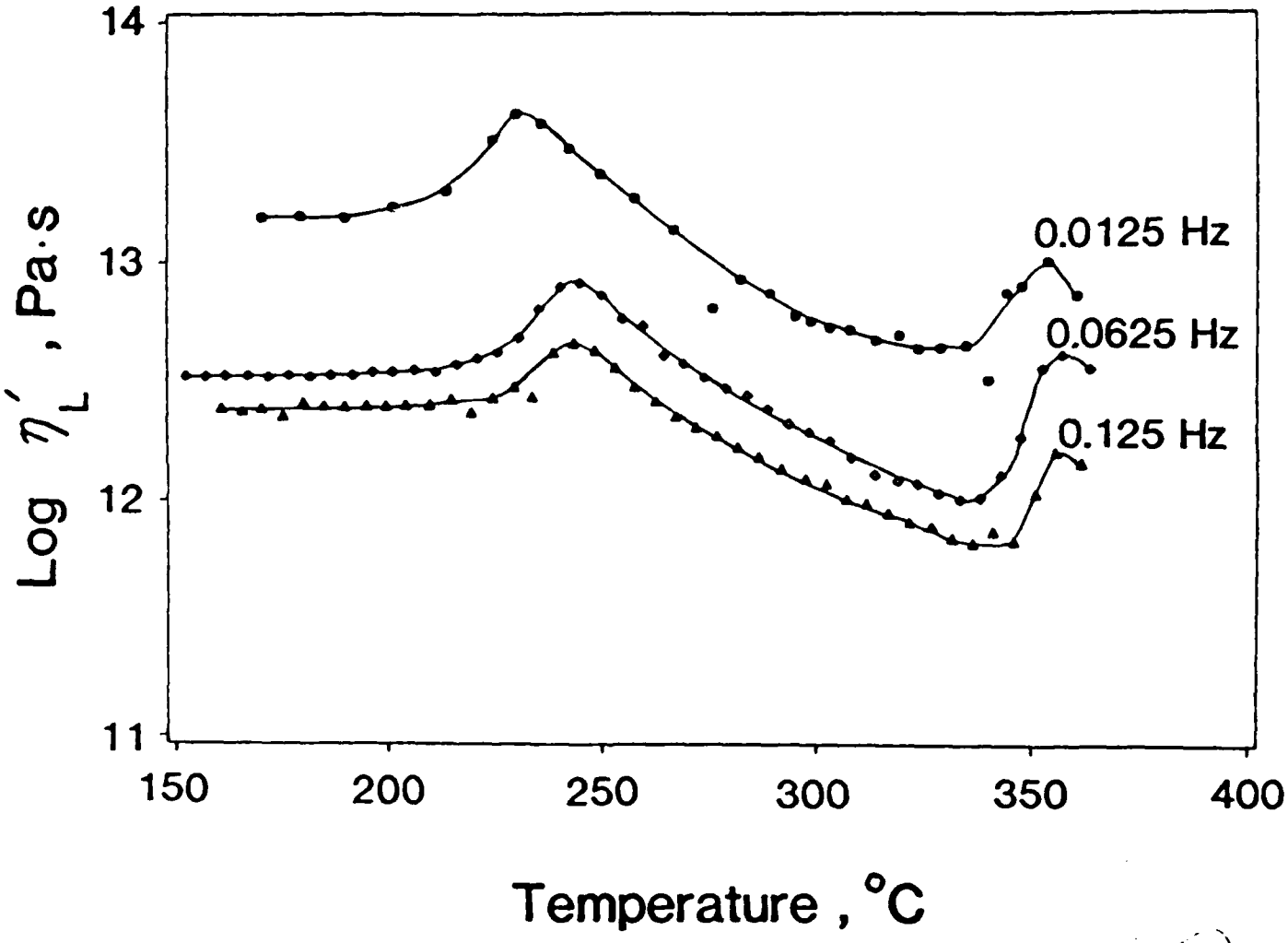
14
13
12
11
Log η_L' , Pa·s
0.0125 Hz
0.0625 Hz
0.125 Hz
150
200
250
300
350
400
Temperature , °C

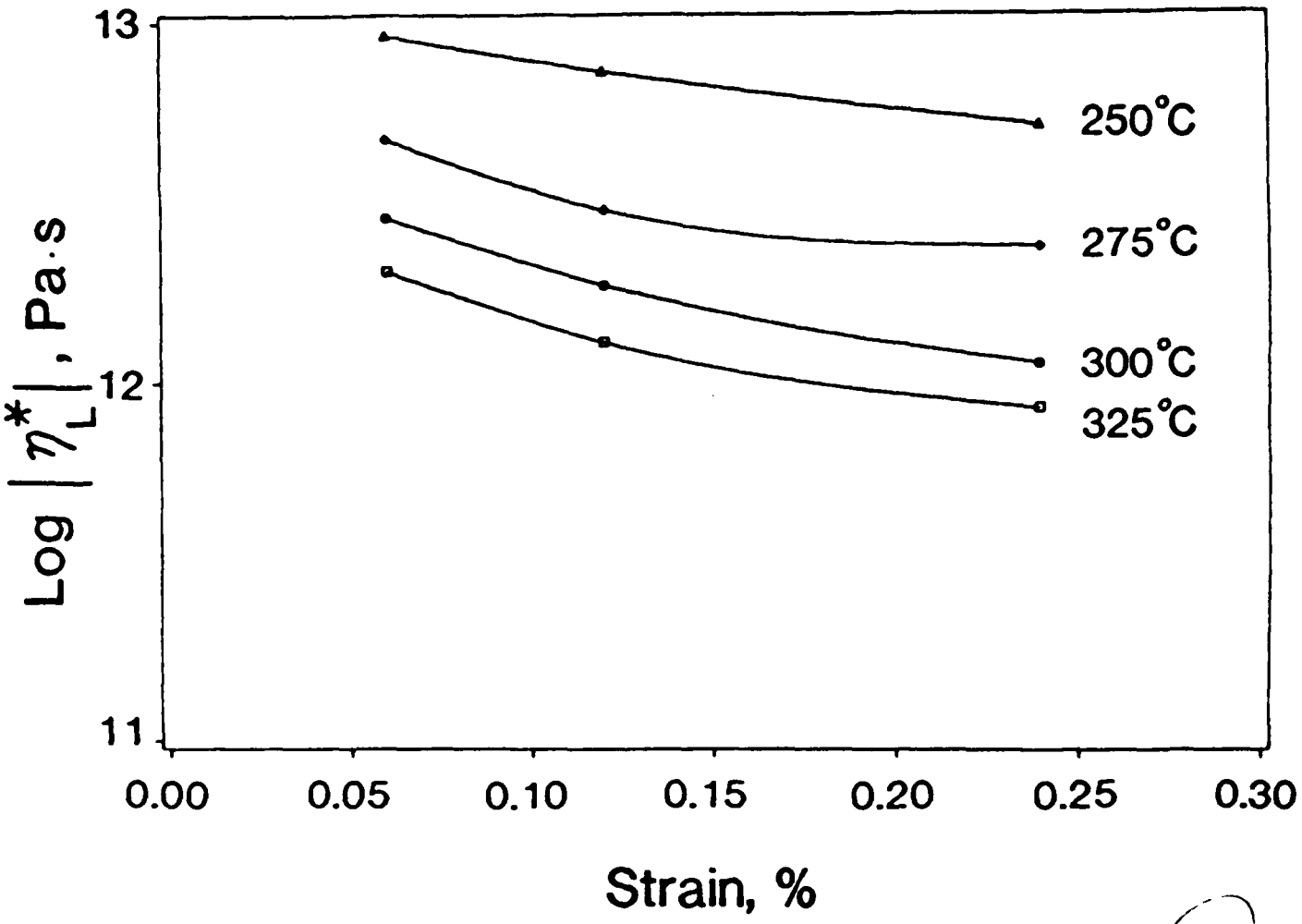
13
12
11
Log $|\eta_L^*|$, Pa·s
250°C
275°C
300°C
325°C
0.00
0.05
0.10
0.15
0.20
0.25
0.30
Strain, %

(10)

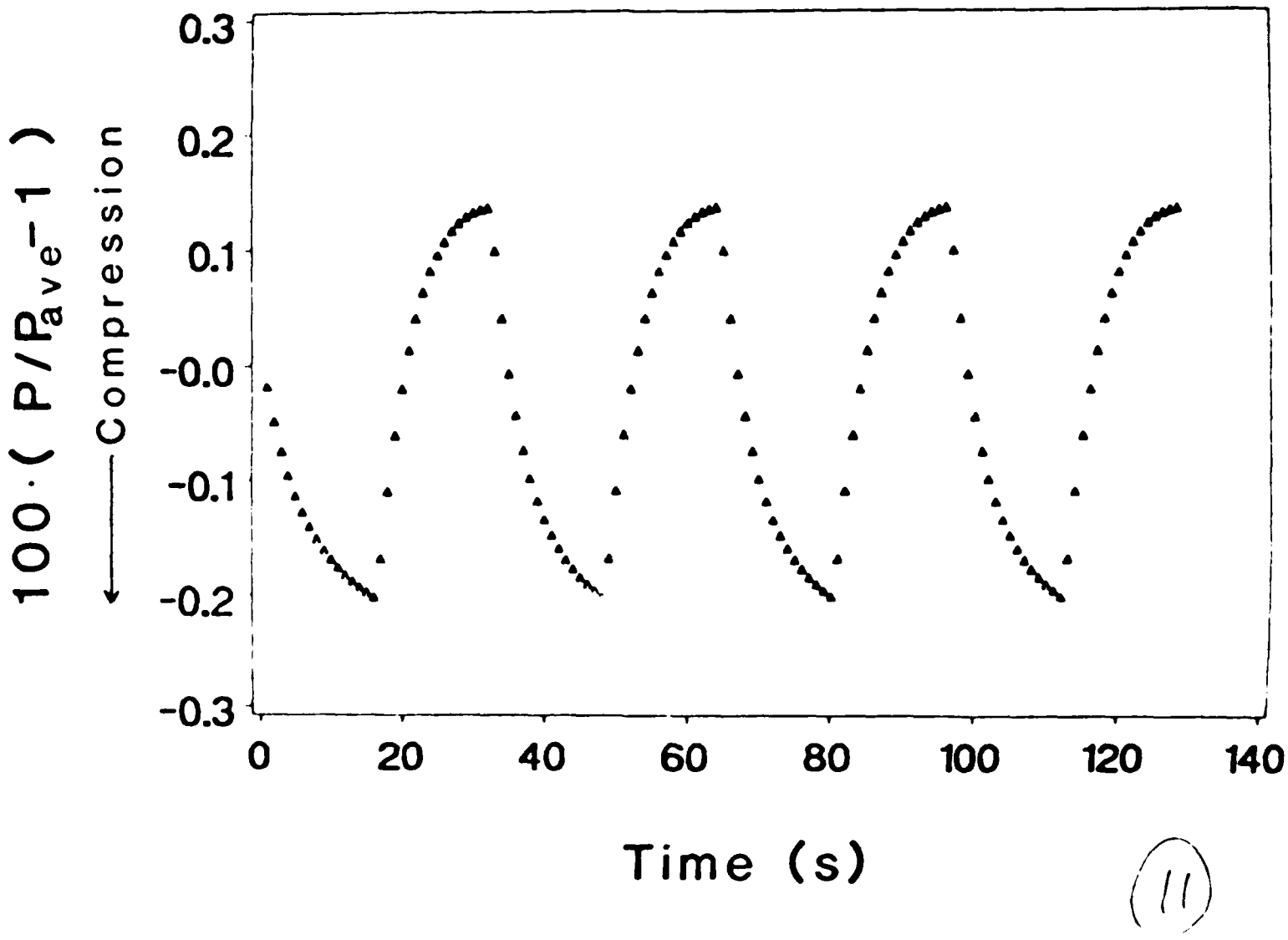
100·(P/Pave−1)
Compression
0.3
0.2
0.1
-0.0
-0.1
-0.2
-0.3
0
20
40
60
80
100
120
140
Time (s)

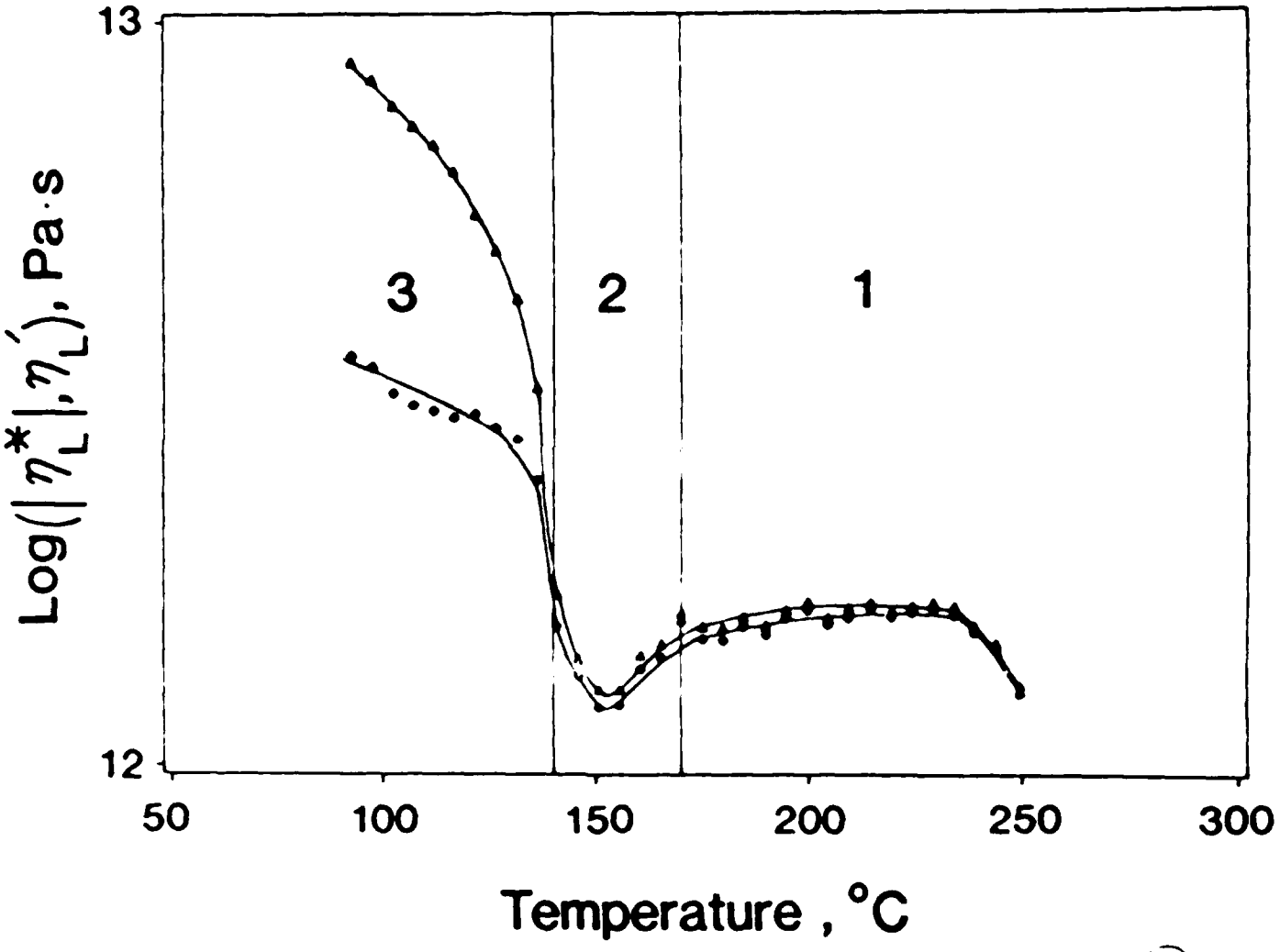
13
12
50
100
150
200
250
300
3
2
1
Log(|η*L|,η'L), Pa·s
Temperature , °C

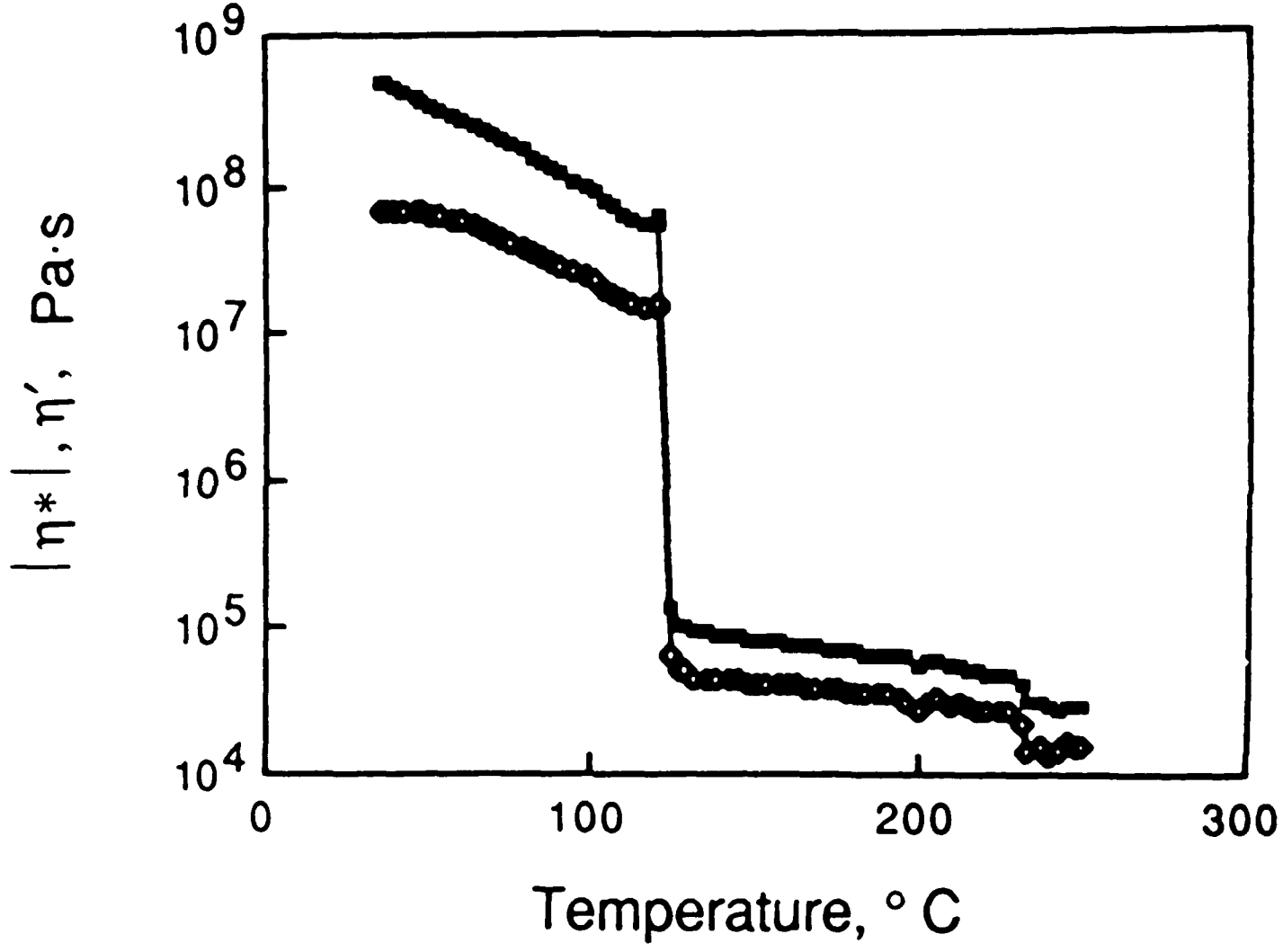

(15)

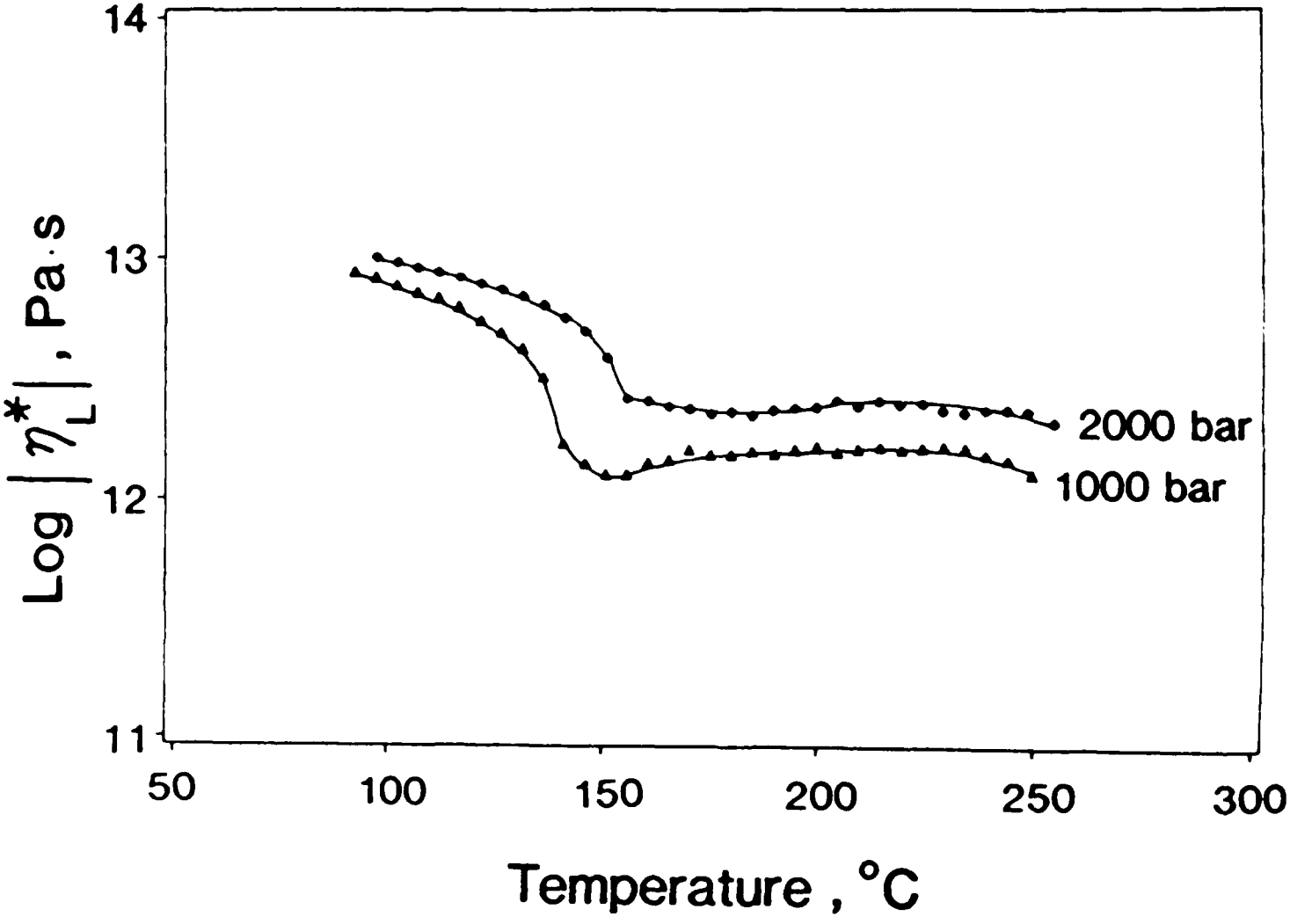
14
13
12
11
Log $|\eta^*_L|$, Pa·s
50
100
150
200
250
300
Temperature , °C
2000 bar
1000 bar

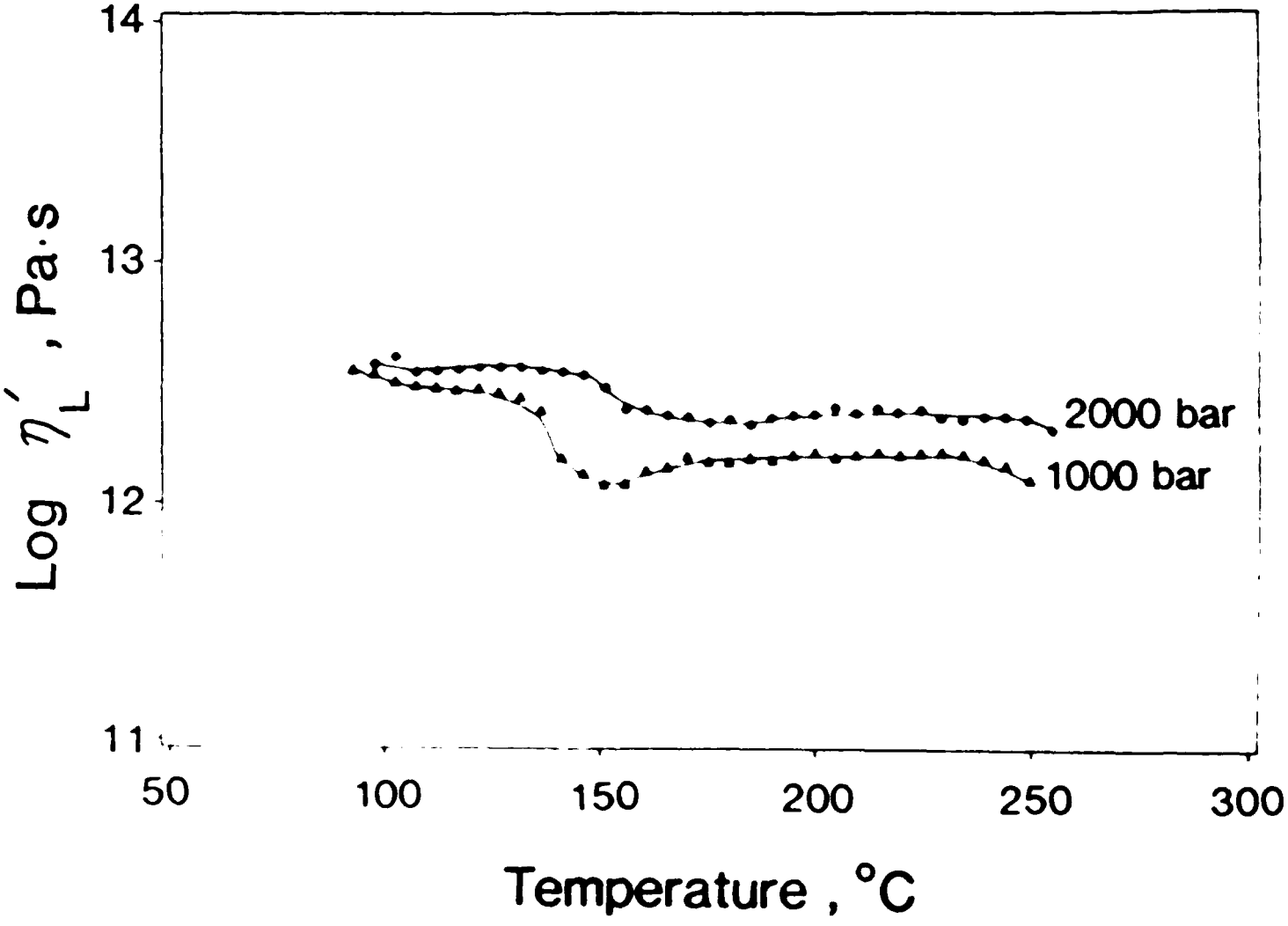
14
13
12
11
Log η_L' , Pa·s
2000 bar
1000 bar
50
100
150
200
250
300
Temperature , °C

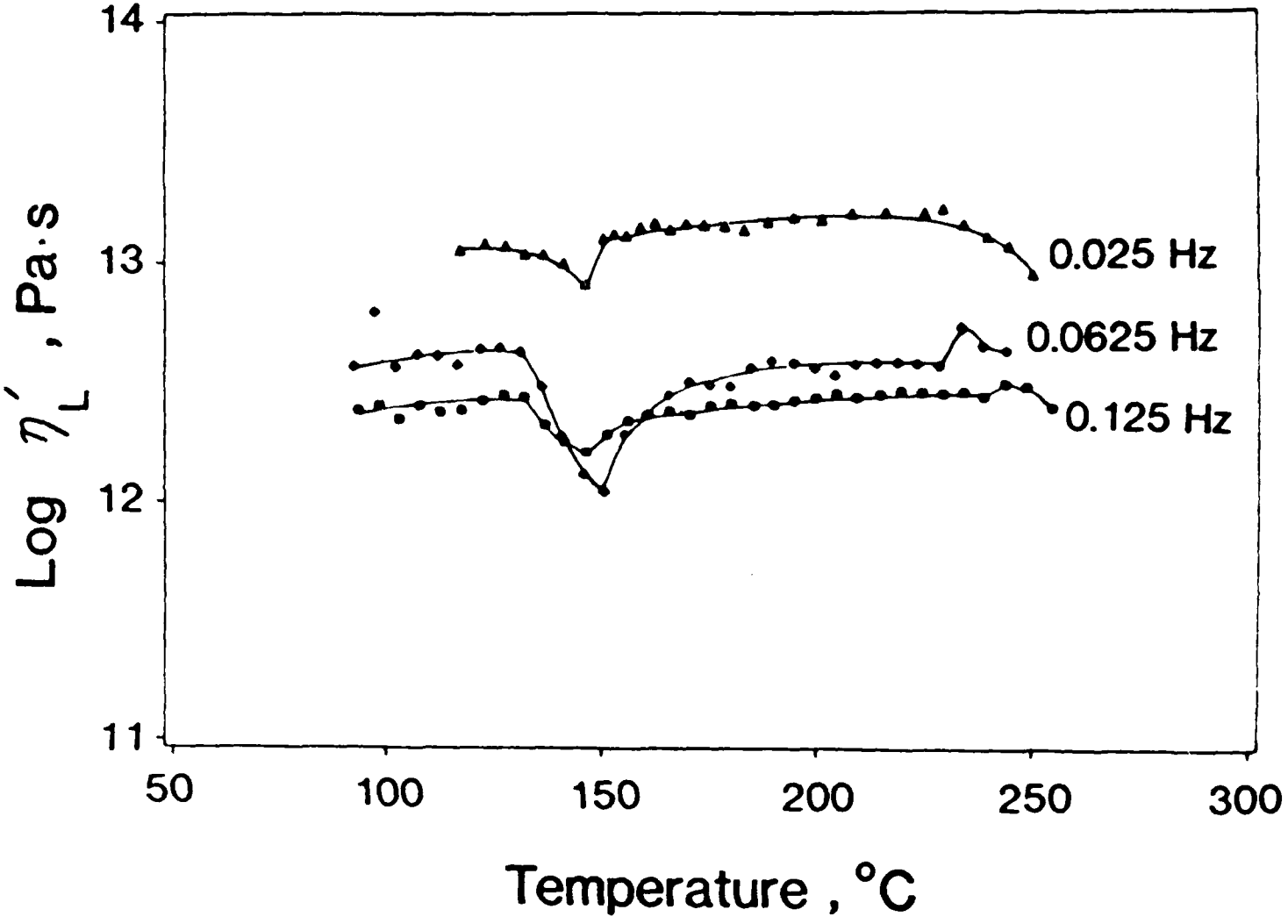
14
13
12
11
Log η_L' , Pa·s
0.025 Hz
0.0625 Hz
0.125 Hz
50
100
150
200
250
300
Temperature , °C

(14)

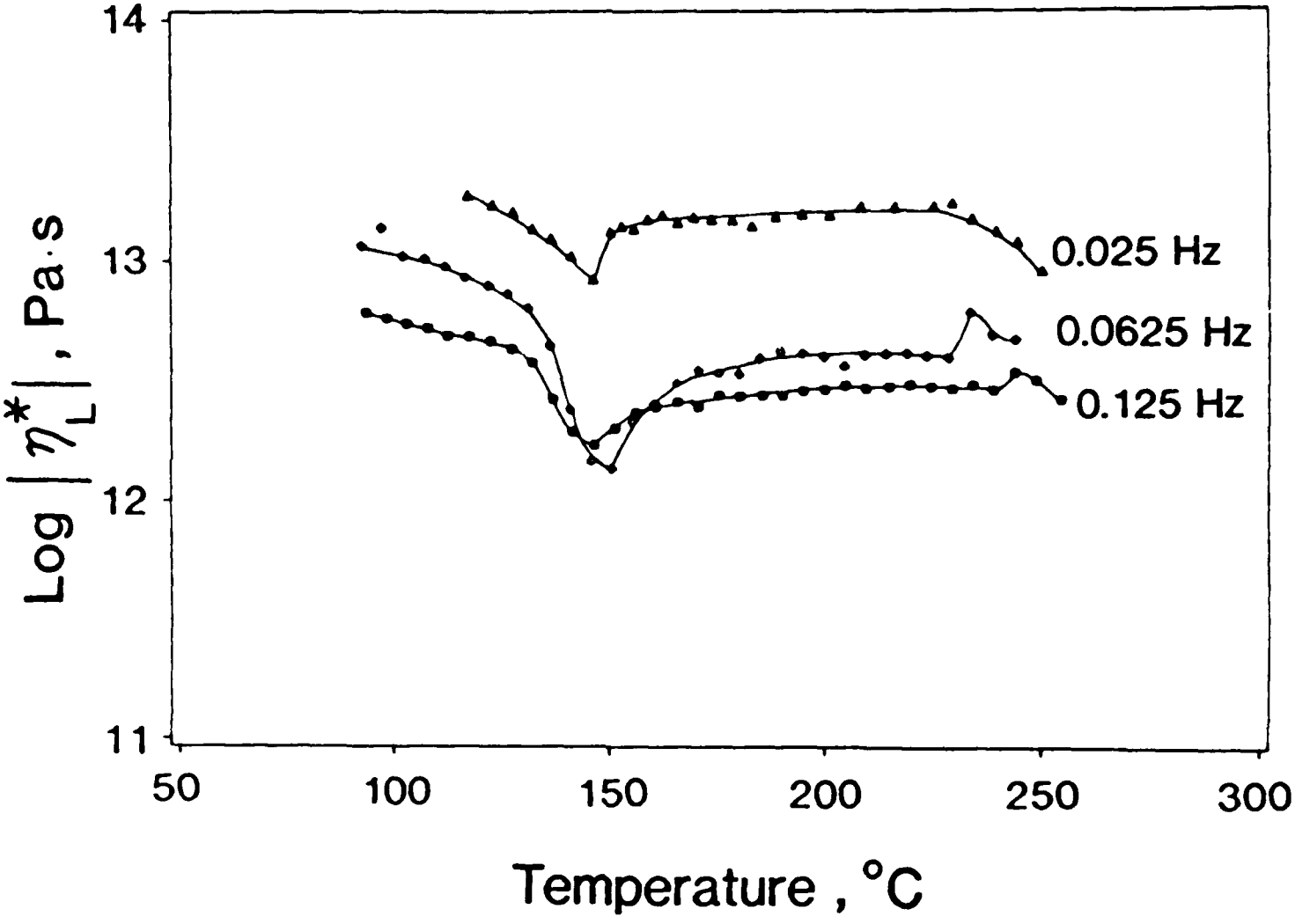
14
13
12
11
50
100
150
200
250
300
Log |η*L|, Pa·s
Temperature , °C
0.025 Hz
0.0625 Hz
0.125 Hz

(17)

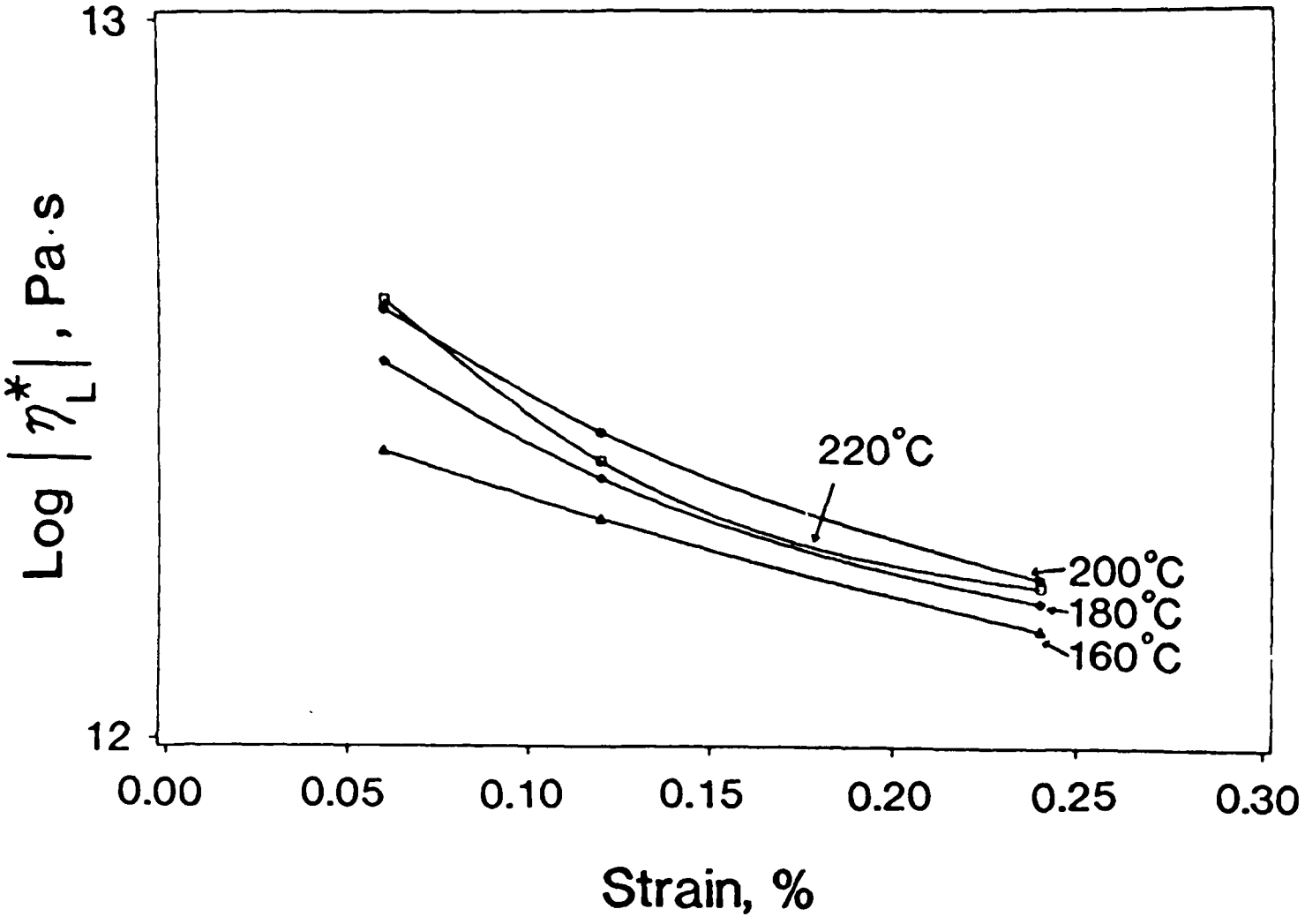
13
12
Log $|\eta_L^*|$, Pa·s
0.00
0.05
0.10
0.15
0.20
0.25
0.30
Strain, %
220°C
200°C
180°C
160°C

DL/1113/87/2

TECHNICAL REPORT DISTRIBUTION LIST, GEN

	No. Copies
Office of Naval Research Attn: Code 1113 800 N. Quincy Street Arlington, Virginia 22217-5000	2
Dr. Bernard Douda Naval Weapons Support Center Code 50C Crane, Indiana 47522-5050	1
Naval Civil Engineering Laboratory Attn: Dr. R. W. Drisko, Code L52 Port Hueneme, California 93401	1
Defense Technical Information Center Building 5, Cameron Station Alexandria, Virginia 22314	12 high quality
DTNSRDC Attn: Dr. H. Singerman Applied Chemistry Division Annapolis, Maryland 21401	1
Dr. William Tolles Superintendent Chemistry Division, Code 6100 Naval Research Laboratory Washington, D.C. 20375-5000	1
Dr. David Young Code 334 NORDA NSTL, Mississippi 39529	1
Naval Weapons Center Attn: Dr. Ron Atkins Chemistry Division China Lake, California 93555	1
Scientific Advisor Commandant of the Marine Corps Code RD-1 Washington, D.C. 20380	1
U.S. Army Research Office Attn: CRD-AA-IP P.O. Box 12211 Research Triangle Park, NC 27709	1
Mr. John Boyle Materials Branch Naval Ship Engineering Center Philadelphia, Pennsylvania 19112	1
Naval Ocean Systems Center Attn: Dr. S. Yamamoto Marine Sciences Division San Diego, California 91232	1

END

9-87

DTIC